Praise Worthy Prize

International Review of Electrical Engineering (I.R.E.E.), Vol. 10, N. 2
ISSN 1827- 6660 March – April 2015

Power Quality Enhancement of Grid Connected Doubly-Fed Induction Generator Using Sliding Mode Control

Riyadh Rouabhi, Rachid Abdessemed, Aissa Chouder, Ali Djerioui

Abstract – *In this paper, we present a simulation study of a wind system with a doubly fed induction machine driven by a variable pitch wind turbine. The objective of the work is to design a control algorithm based on the sliding mode control strategy allowing the control of both active and reactive power independently. The main goal achieved by the control strategy is to control the amount of active and reactive power produced by the doubly fed induction generator and injected in the main grid according to the power references derived from turbine's mechanical power and the grid operator. The simulation results have shown good performances concerning the tracking of the references both in transient and steady state.*
A comparative study between the proposed control strategy and the well known vector control strategy has been carried out and has shown the superiority of sliding mode control to track the given references.

Keywords: *Bidirectional Converter, Doubly Fed Induction Machine, Maximum Power Point Tracking (MPPT), Modeling Of Wind System, Vector Control, Sliding Mode Control*

I. Introduction

Nowadays wind based energy generation is gaining more and more visibility in a context of an increasing power demand worldwide [1]. The merit of wind energy is mainly due to its economic viability compared with conventional energy and especially the clean nature of the energy production process allowing the mitigation of dioxyde carbon emissions [2].

However, the stochastic nature of the primary source from one hand and the grid utlity requirements in term of power quality on the other hand have lead to a massive penetration of power converters as an interface to improve the electrical variables shaping at the point of common coupling (PCC). Therefore, proper integration of wind turbine based energy generation into the grid utility require a detailed modeling process of wind turbine, power converters and the associated control strategies [3]-[4]. During the last decade, wind farms based on doubly fed induction generator (DFIG) technology are becoming more attractive and very popular due to its advantages compared with others generators such as variable speed and constant frequency operation, decoupled active/reactive power control, maximum power tracking capability, reduced dimension of the static converter (AC/AC) to about 25%-30% of the generator rating which led to lower converter's cost and lower power losses [5]-[6]-[7]-[8].

Many research papers have addressed the issue of power quality enhancement of DFIG wind energy system based on the stator's active and reactive power control.

Vector control approaches are widely used due to their ability to handle the decoupled model of the DFIG [9].

However vector control approche exhibits low performance and less robustness when the DFIG nonlinearities are considered.

Thus, nonlinear control strategies such as sliding mode control have been more attractive due their inherent properties to deal with unmodeled dynamics, insensitivity to parameters variation, disturbance rejection and fast dynamic response. These properties are suitable for controlling both active and reactive power generated by a wind energy conversion system (WECS) based on a DFIG connected to the grid utility [10]-[12].

In this paper a sliding mode control strategy applied to a DFIG wind energy conversion system is proposed. First the different components of a wind energy system are modeled. Then, a combination of vector control and sliding mode control to enhance the tracking capabilities of the reference active and reactive powers respectively.

In the second stage, a simulation study is carried out using Matlab/Simulink environment, to verify the effectiveness of the proposed control algorithms.

The paper is structured as follows. Section 1 describes the wind turbine modeling details. Section 2 presents the different components of a wind energy system and their modeling procedure. Section 3 focuses on the structure of the vector control for controlling independently active and reactive powers.

In section 4 it is given the design of the proposed sliding mode (SM) based on the active and reactive powers derivation.

Section 5 gives the numerical simulation results and discussion. Finally, Section 6 provides a conclusion of the present work.

II. System Description

The studied wind system based on DFIG is mainly composed by a wind turbine, doubly fed induction generator and bidirectional power converter. A model of each sub-system is shown in Fig. 1.

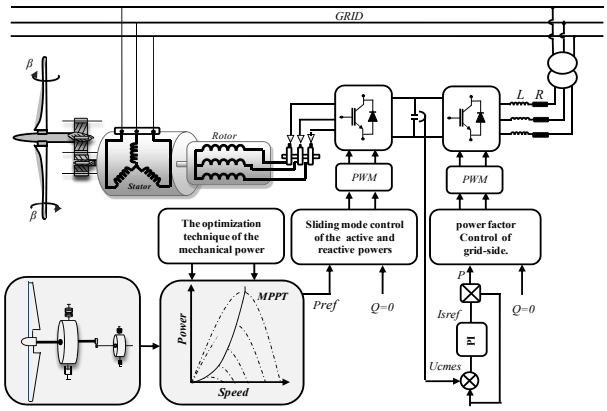

Fig. 1. Global configuration of the wind energy conversion systems

III. Modeling and Control of the Individual Components of Wind System

III.1. Modeling and Control of the Turbine

Modeling of the turbine

The turbine is made up of three-bladed rotor and a hub. Through the turbine, wind energy is transformed into mechanical energy that rotate the main shaft of the generator. The aerodynamic (mechanical) power P_m extracted by the wind turbine is given by [13]:

$$P_m = \frac{1}{2}\cdot\rho\cdot\pi\cdot R_T^2\cdot V^3\cdot C_p(\lambda,\beta) \tag{1}$$

where ρ is the air density, R_T is the wind turbine rotor length, V is the wind speed. The power coefficient Cp (λ, β) represents the turbine efficiency to convert the kinetic energy of the wind into mechanical energy. This coefficient is a function of both the blade pitch angle β and the tip speed ratio λ, which is defined as [14]:

$$\lambda = \frac{\Omega_T\cdot R_T}{V} \tag{2}$$

where Ω_T is the shaft speed in (rad/s).

As a matter of example, the expression of the power coefficient of a wind turbine of 4 kW is approximated by the following equation. Fig. 2 shows the plot of $Cp(\lambda,\beta)$ as function of both lambda and beta:

$$\begin{aligned} C_p(\lambda,\beta) = &\left(0{,}5-0{,}167.(\beta-2)\right)\cdot \\ &\cdot sin\left[\frac{\pi.(\lambda+0{,}1)}{18{,}5-0{,}3.(\beta-2)}\right]+ \\ &-0{,}00184.(\lambda-3)\cdot(\beta-2) \end{aligned} \tag{3}$$

$$\begin{aligned} &C_g = \frac{C_T}{G},\ \Omega_T = \frac{\Omega_g}{G} \\ &\frac{C_T}{G} - C_g = J\cdot\frac{d\Omega_g}{dt} + f\cdot\Omega_g \end{aligned} \tag{4}$$

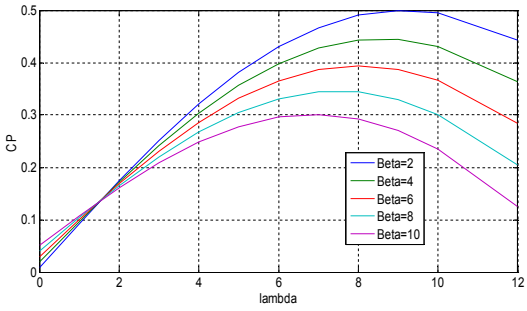

Fig. 2. Power coefficient Cp according to λ for different β

Ideal characteristics of a wind turbine at variable speed

Zone I: corresponds with the low speed of the insufficient wind to actuate the wind system. The objective in this zone is to extract the maximum of power of the wind by applying techniques called extraction of maximum of power.

Zone II: in this zone, the speed of the wind is constant.

Zone III: corresponds with the very high speed of the wind, the objective in this zone is to limit the output power to a value equal to the nominal power of the wind system to avoid overloads. This is done by action on the pitch angle of the blades [15].

Control in lower part of the nominal output (optimization of the power)

In this zone of operation, the control has as main objectives to maximize the captured energy of the wind and to minimize the efforts undergone by the driving mechanism. To maximize the capture of wind energy, there are two variables which are controlled in order to be maintained at their optimal values namely: Cp_{max} = (λopt, βopt). B is maintained by fixing the pitch angle at its optimal value βopt, and λ by fixing the specific speed to its optimal value. The characteristic corresponding to this relation is given in Zone *I* of Figs. 3.

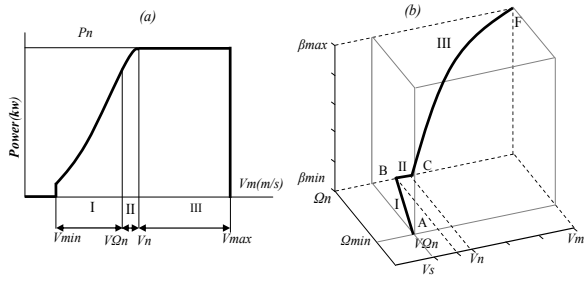

Figs. 3. Ideal characteristic of a wind turbine at variable speed

Indirect control in Zone I

The optimization technique of the mechanical power used in this zone is the Maximum Power Point Tracking

Control (MPPT). In the present work, maximum power coefficient is taken as: $C_{p\ max}$=0.48 by achieving for a tip speed ratio of λ_{opt} =9.2 and β=2 deg.

This choice has been dictated according to Fig. 2 [16]:

$$C_{Topt} = \frac{1}{2}\cdot\rho\cdot\pi\cdot R_T^3\cdot V^2\,\frac{C_p\left(\lambda_{opt}\right)}{\lambda_{opt}} \tag{5}$$

$$V = \frac{R_T\cdot\Omega_T}{\lambda_{opt}} \tag{6}$$

$$C_{Topt} = \frac{1}{2}\cdot\rho\cdot\pi\cdot R_T^5\cdot\frac{C_p\left(\lambda_{opt}\right)}{\lambda_{opt}^3}\cdot\Omega_T^2 \tag{7}$$

$$C_{Topt} = k_{opt}\cdot\Omega_T^2 \quad \text{and} \quad k_{opt} = \frac{1}{2}\cdot\rho\cdot\pi\cdot R_T^5\cdot\frac{C_p\left(\lambda_{opt}\right)}{\lambda_{opt}^3}$$

$$\frac{C_T}{G} - C_g - f\cdot\Omega_g = 0 \quad \text{and} \quad \frac{k_{opt}}{G}\cdot\Omega_T^2 - f\cdot\Omega_g - C_g = 0$$

with:

$$\Omega_g = G\cdot\Omega_T \quad \text{then} \quad C_{gopt} = \frac{k_{opt}}{G^3}\cdot\Omega_g^2 - f\cdot\Omega_g$$

The block diagram given by the Fig. 4 shows the implementation of the indirect control of the turbine.

III.2. Modeling of the Generator

A classical modeling of the doubly fed induction generator in the Park reference frame is used.

The voltage and flux equations of the DFIG are given as follows in Eq. (8) [17]-[20], [30]-[32]:

$$\begin{cases} V_{sd} = R_s I_{sd} + \dfrac{d\varphi_{sd}}{dt} - w_s\varphi_{sq} \\ V_{sq} = R_s I_{sq} + \dfrac{d\varphi_{sq}}{dt} + w_s\varphi_{sd} \\ V_{rd} = R_r I_{rd} + \dfrac{d\varphi_{rd}}{dt} - w_r\varphi_{rq} \\ V_{rq} = R_r I_{rq} + \dfrac{d\varphi_{rq}}{dt} + w_r\varphi_{rd} \end{cases} \text{ and } \begin{cases} \varphi_{sd} = L_s I_{sd} + M I_{rd} \\ \varphi_{sq} = L_s I_{sq} + M I_{rq} \\ \varphi_{rd} = L_r I_{rd} + M I_{sd} \\ \varphi_{rq} = L_r I_{rq} + M I_{sq} \end{cases}$$

The electromagnetic torque equation is given by:

$$C_{em} = p\frac{M}{L_s}\left(I_{rd}\varphi_{sq} - I_{rq}\varphi_{sd}\right) \tag{9}$$

The stator active and reactive powers are expressed by:

$$\begin{cases} P = V_{sd} I_{sd} + V_{sq} I_{sq} \\ Q = V_{sq} I_{sd} - V_{sd} I_{sq} \end{cases} \tag{10}$$

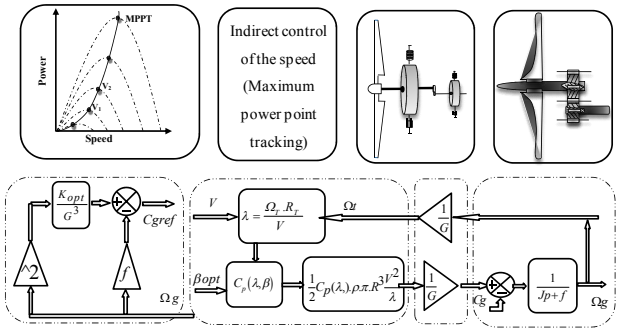

Fig. 4. Diagram block of the turbine's model and indirect control speed (Zone I)

In the state space representation, the system is given as:

$$\left[\dot{X}\right] = [A]\cdot[X] + [B]\cdot[U] \tag{11}$$

with:

$$[X] = \begin{bmatrix} \varphi_{sd} & \varphi_{sq} & i_{rd} & i_{rq} \end{bmatrix}^t$$

$$[U] = \begin{bmatrix} v_{sd} & v_{sq} & v_{rd} & v_{rq} \end{bmatrix}^t$$

$$[A] = \begin{bmatrix} \dfrac{-1}{T_s} & \text{Where: } w_s & \dfrac{M}{T_s} & 0 \\ -w_s & \dfrac{-1}{T_s} & 0 & \dfrac{M}{T_s} \\ \alpha & -\beta w_e & -\delta & w_r \\ \beta w_e & \alpha & -w_r & -\delta \end{bmatrix}$$

$$[B] = \begin{bmatrix} 1 & 0 & 0 & 0 \\ 0 & 1 & 0 & 0 \\ \dfrac{-M}{\sigma L_r L_s} & 0 & \dfrac{1}{\sigma L_r} & 0 \\ 0 & \dfrac{-M}{\sigma L_r L_s} & 0 & \dfrac{1}{\sigma L_r} \end{bmatrix}$$

α , β and δ are constants defined as follows:

$$\alpha = \frac{M}{\sigma T_s L_s L_r} \qquad \beta = \frac{M}{\sigma L_s L_r}$$

$$\delta = \frac{1}{\sigma}\left(\frac{1}{T_r} + \frac{M^2}{T_s L_r L_s}\right); \qquad w_e = w_s - w_r$$

III.3. Modeling and Control of the Grid Side Converter

The Grid side converter is used to provide bi-directed power flow from rotor-side converter allowing the

stabilization of the DC-link voltage and achieving unity power factor.

Modeling of the grid side converter

The AC source model and the rectifier model are given by the state space representation:

$$\frac{d}{dt}\begin{bmatrix} i_1 \\ i_2 \\ i_3 \end{bmatrix} = \begin{bmatrix} -\frac{R}{L} & 0 & 0 \\ 0 & -\frac{R}{L} & 0 \\ 0 & 0 & -\frac{R}{L} \end{bmatrix}\begin{bmatrix} i_1 \\ i_2 \\ i_3 \end{bmatrix} + \frac{1}{L}\begin{bmatrix} V_1 - V_{an} \\ V_2 - V_{bn} \\ V_3 - V_{cn} \end{bmatrix} \quad (12)$$

The Converter:

$$\begin{bmatrix} V_A \\ V_B \\ V_C \end{bmatrix} = \frac{Uc}{3}\cdot\begin{bmatrix} 2 & -1 & -1 \\ -1 & 2 & -1 \\ -1 & -1 & 2 \end{bmatrix}\begin{bmatrix} S_1 \\ S_2 \\ S_3 \end{bmatrix} \quad (13)$$

In addition, the rectified current is given by:

$$i_s = \begin{bmatrix} S_1 & S_2 & S_3 \end{bmatrix}\begin{bmatrix} i_1 \\ i_2 \\ i_3 \end{bmatrix} \quad (14)$$

The output voltage is governed by:

$$\frac{dU_C}{dt} = \frac{1}{C}\left(i_s - i_L\right) \quad (15)$$

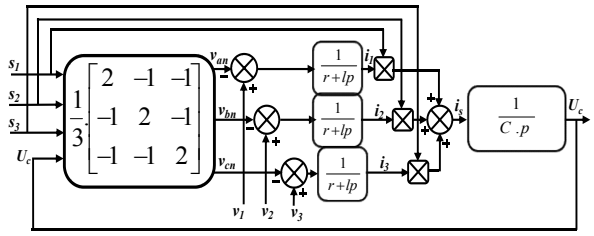

Fig. 5. Schematic diagram of grid side converter

Grid side converter controller design

The objective of the grid side converter is to regulate the DC link voltage and to set a unit power factor.

The equations allowing the expression of the input AC voltage $Vp(d,q)$ to the rectifier in the (d,q) frame as a function of the voltages at the common connection point (CCP), $V(d,q)$ are given by the following equations:

$$\begin{cases} V_{pd} = V_d - R\cdot i_d - L\dfrac{di_d}{dt} + Lw\cdot I_q \\ V_{pq} = V_q - R\cdot i_q - L\dfrac{di_q}{dt} - Lw\cdot I_d \end{cases} \quad (16)$$

The real and reactive powers are expressed by:

$$\begin{cases} P = \dfrac{3}{2}\left[V_d I_d + V_q I_q\right] \\ Q = \dfrac{3}{2}\left[V_q I_d + V_d I_q\right] \end{cases} \quad (17)$$

which can be rewritten in grouped form as:

$$\begin{bmatrix} P \\ Q \end{bmatrix} = \frac{3}{2}\cdot\begin{bmatrix} V_d & V_q \\ V_q & -V_d \end{bmatrix}\begin{bmatrix} I_d \\ I_q \end{bmatrix} \quad (18)$$

Eq. (19) allows us processing the reference currents ($I^*_{d,q}$) knowing the active and reactive powers references (P^*, Q^*):

$$\begin{bmatrix} I^*_d \\ I^*_q \end{bmatrix} = \frac{2}{3\left(V_d{}^2 + V_q{}^2\right)}\begin{bmatrix} V_d & V_q \\ V_q & -V_d \end{bmatrix}\begin{bmatrix} P^* \\ Q^* \end{bmatrix} \quad (19)$$

where V_d, V_q are the actual measured grid voltages.

The reference of the real power P^* is calculated from the DC bus control loop responsible of maintaining constant DC capacitor voltage. Its value given by the following expression:

$$P^* = U_c I_s \quad \text{and} \quad Q^* = 0$$

The diagram block of the regulation is then represented in the figure below.

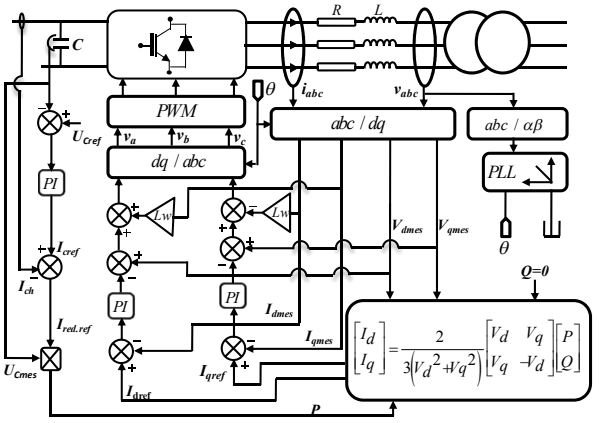

Fig. 6. Bloc diagram of the grid side converter control

III.4. Modeling of the Rotor Side Converter

The rotor side converter is used to control the active and reactive powers injected by the stator of the doubly fed induction generator to the grid.

The converter used is a simple three-phase inverter on two levels (six switches). The mathematical model of the rotor side converter:

$$\begin{bmatrix} V_A \\ V_B \\ V_C \end{bmatrix} = \frac{E}{6}\cdot\begin{bmatrix} 2 & -1 & -1 \\ -1 & 2 & -1 \\ -1 & -1 & 2 \end{bmatrix}\begin{bmatrix} S_1 \\ S_2 \\ S_3 \end{bmatrix} \quad (20)$$

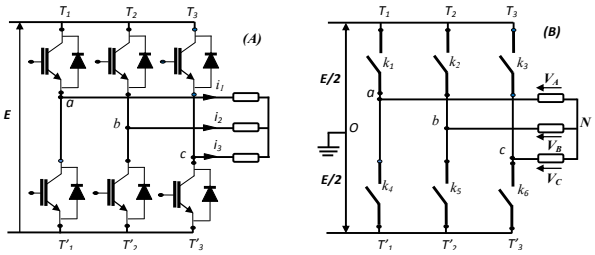

Figs. 7. Schematic diagram of rotor side converter

IV. Vector Control of the Active and Reactive Powers

Vector control allows to separately controlling the active and reactive power flow between utility grid and wind generator [21]. Stator and rotor variables are both referred to Park's stator reference frame.

With this orientation, the d-component of the stator flux is equal to the total flux while the *q*-component is equal to zero i.e $\varphi_{sd} = \varphi_s$ and $\varphi_{sq} = 0$.

Using this approach, a decoupled control between the stator's active and reactive powers can be then obtained [22]. Assuming the windings stator resistance R_s is neglected and referring to the chosen reference frame, the voltage and the flux equations of the stator winding can be simplified in steady state as follows [23]:

$$\begin{cases} V_{sd} = 0 \\ V_{sq} = V_s = w_s \cdot \varphi_s \\ V_{rd} = R_r \cdot I_{rd} + \dfrac{d\varphi_{rd}}{dt} - w_r \varphi_{rq} \\ V_{rq} = R_r \cdot I_{rq} + \dfrac{d\varphi_{rq}}{dt} + w_r \varphi_{rd} \end{cases} \quad (21)$$

and the equations of flux are expressed by:

$$\begin{cases} \varphi_{sd} = \varphi_s = L_s \cdot I_{sd} + M \cdot I_{rd} \\ 0 \quad = L_s \cdot I_{sq} + M \cdot \varphi_{rq} \\ \varphi_{rd} = L_r \cdot I_{rd} + M \cdot \varphi_{sd} \\ \varphi_{rq} = L_r \cdot I_{rq} + M \cdot \varphi_{sq} \end{cases} \quad (22)$$

The relationship between stator powers and rotor currents are given by the following equations:

$$\begin{cases} P_s = -\dfrac{V_s \cdot M}{L_s} \cdot I_{rq} \\ Q_s = \dfrac{V_s^2}{w_s \cdot L_s} - \dfrac{V_s \cdot M}{L_s} I_{rd} \end{cases} \quad (23)$$

$$\begin{cases} I_{rq} = -\dfrac{L_s}{V_s \cdot M} \cdot P_s \\ I_{rd} = \dfrac{V_s^2}{w_s \cdot L_s} - \dfrac{L_s}{V_S \cdot M} \cdot Q_s \end{cases} \quad (24)$$

The obtained control voltages which will drive the rotor are given by the following expressions:

$$\begin{cases} V_{rd} = \left[R_r + \left(L_r - \dfrac{M^2}{L_s} \right) s \right] I_{rd} + \\ \qquad -g \cdot w_s \left(L_r - \dfrac{M^2}{L_s} \right) \cdot I_{rq} \\ V_{rq} = \left[R_r + \left(L_r - \dfrac{M^2}{L_s} \right) s \right] I_{rq} + \\ \qquad +g \cdot w_s \left(L_r - \dfrac{M^2}{L_s} \right) \cdot I_{rd} + g \cdot \dfrac{V_s \cdot M}{L_s} \end{cases} \quad (25)$$

In Fig. 8, it is give the block diagram of vector control approach applied to the DIFG.

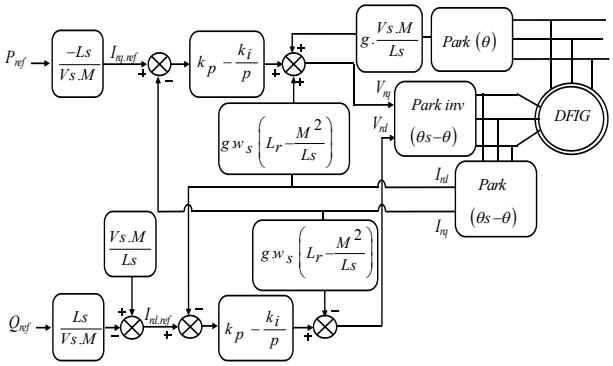

Fig. 8. Block diagram of oriented stator flux of a voltage controlled DFIG

V. Sliding Mode Control of the Active and Reactive Powers

Sliding Mode Controller (SMC) is a powerful nonlinear controller which has been analysed by many researchers especially in recent years [33]-[35]. This method forces the system to slide along a predesigned sliding mode surface and alters the dynamic of system by using a discontinuous control signal [24].

Sliding mode (SM) control possesses strengthen robustness and has been successfully applied in wind energy conversion system (WECS) [25]. In this paper, a controller is designed for a decoupled control strategy of the active and reactive power based on the sliding mode algorithm to match WECS variable environments.

Thus, the relationships between stator powers and rotor currents are given by:

$$\begin{aligned} I_{rq}^{ref} &= -\frac{L_s}{V_s \cdot M} \cdot P_s^{ref} \\ I_{rd}^{ref} &= \frac{V_s}{w_s \cdot M} - \frac{L_S}{V_S \cdot M} \cdot Q_s^{ref} \end{aligned} \quad (26)$$

The derivative rotor currents are then given by:

$$\begin{cases} \dfrac{dI_{rd}}{dt} = \begin{pmatrix} V_{rd} - R_r \cdot I_{rd} + \\ +g \cdot w_s \cdot L_r \cdot \sigma \cdot I_{rq} \end{pmatrix} \cdot \dfrac{1}{L_r \sigma} \\ \dfrac{dI_{rq}}{dt} = \begin{pmatrix} V_{rq} - R_r \cdot I_{rq} - g \cdot w_s \cdot L_r \\ \cdot \sigma \cdot I_{rd} - g \cdot w_s \cdot \dfrac{M \cdot V_s}{w_s \cdot L_s} \end{pmatrix} \cdot \dfrac{1}{L_r \sigma} \end{cases} \quad (27)$$

V.1. Sliding Mode Controller Design

Design of sliding mode controller takes into consideration system stability and accounts for stability and good performances in a systematic way. Here after, detailed design steps of the sliding mode controller are given:

Choice of the sliding surfaces

The first phase of the control design consists of choosing the number of the switching surfaces *s(x)*. Generally this number is equal to the dimension of the control vector [*V*] [26].

The active power is directly proportional to the rotor current in the *q axis* while reactive power is proportional to the rotor current in *d axis*. Thus, the expression of the control surfaces of active and reactive powers is given by:

$$s(P) = \left(I_{rq}^{ref} - I_{rq} \right) \quad (28)$$

$$s(Q) = \left(I_{rd}^{ref} - I_{rd} \right) \quad (29)$$

Conditions of convergence

In order to ensure to convergence to the references variables, it is necessary that the two sliding surfaces must given above must be equal to zero. Therefore, the system of equations given bellow must be verified:

$$\begin{cases} s(P) = 0 \\ \\ s(Q) = 0 \end{cases} \Rightarrow \begin{cases} \dfrac{d}{dt}\left(I_{rq}^{ref} - I_{rq} \right) = 0 \\ \dfrac{d}{dt}\left(I_{rd}^{ref} - I_{rd} \right) = 0 \end{cases} \quad (30)$$

Consequently, for a zero sliding surface s(*P,Q*), the active and reactive power would converge exponentially towards their references.

So, to track Ps^{ref} and Qs^{ref}, it is sufficient making the sliding surface attractive and invariant.

The effectiveness of a sliding mode control is conditioned by checking Lyaponov' attractivity relationship [27], given by:

$$s(X) \cdot \dot{s}(X) \le 0 \quad (31)$$

Sliding mode control algorithm

The third phase consists to derive the control laws which allow the controlled variables to be kept very close to the sliding surface [26]. In order to obtain good dynamic performances, the control voltage vectors are given by the following expressions [28]:

$$\begin{cases} V_{rq} = V_{rq-Equi} + V_{rq-attr} \\ \\ V_{rd} = V_{rd-Equi} + V_{rd-attr} \end{cases} \quad (32)$$

$$\begin{cases} V_{rq-attr} = -k_1 \cdot sgn\left(s(p) \right) \\ \\ V_{rd-attr} = -k_2 \cdot sgn\left(s(Q) \right) \end{cases} \quad (33)$$

V_{rd}, V_{rq}: is the control vector
V_{rd_Equi}, V_{rq_Equi}: is the equivalent control vector
V_{rd_attr}, V_{rq_attr}: is the switching part of the control

Sliding Mode control is a discontinuous control in nature.

So, in order to reduce the chattering effect, a continuous function expressed by Eq.(34) which delimitate the maximum and minimum excursion values of the controlled variables by using a sign function, (*sgn*(*s*(*x*)) defined as follow [29]:

$$sgn\left(S(x) \right) = \begin{cases} -1 & \text{if} \quad S(x) < 0 \\ 1 & \text{if} \quad S(x) > 0 \end{cases} \quad (34)$$

$$V_{rdq-attr} = k_x \frac{S(x)}{|S(x)| + \xi_x} \quad (35)$$

where:
k_x is a constant and
ξ_x is small positive scalar.

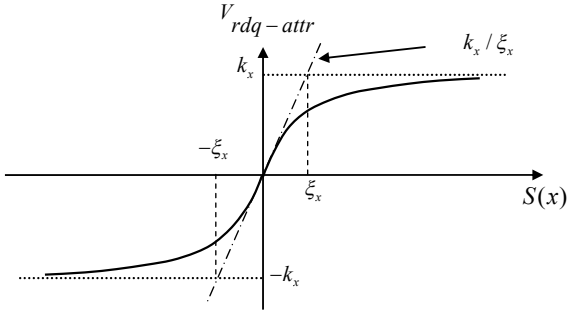

Fig. 9. Shape of the sgn(s(x)) function

V.2. Active Power Control

To control active power, we put r =1(*relative degree of the number of derivative times of the control surface to*

get the control law), so the expression of the control surface and its derivative to control active power are given by:

$$s(P)=\left(I_{rq}^{ref}-I_{rq}\right) \tag{36}$$

$$\dot{s}(P)=\left(\dot{I}_{rq}^{ref}-\dot{I}_{rq}\right) \tag{37}$$

By replacing $\dot{I}_{rq}^{ref}$ and $\dot{I}_{rq}$ by their relative expressions, we get:

$$\dot{s}(P)=\begin{pmatrix}-\dfrac{L_s}{M\cdot V_s}\cdot\dot{P}_s^{ref}-\dfrac{1}{L_r\sigma}\cdot\\ \begin{pmatrix}V_{rq}-R_r\cdot I_{ç}-g\cdot w_s\cdot L_r\cdot\sigma\cdot I_{rd}+\\ -g\cdot\dfrac{M\cdot V_s}{L_s}\end{pmatrix}\end{pmatrix} \tag{38}$$

$$\dot{s}(P)=\begin{pmatrix}-\dfrac{L_s}{M\cdot V_s}\cdot\dot{P}_s^{ref}-\dfrac{1}{L_r\sigma}\cdot V_{rq}-\dfrac{1}{L_r\sigma}\cdot\\ \left(-R_r\cdot I_{rq}-g\cdot w_s\cdot L_r\cdot\sigma\cdot I_{rd}-g\cdot\dfrac{M\cdot V_s}{L_s}\right)\end{pmatrix} \tag{39}$$

$$\begin{aligned}V_{rq}=&-\frac{L_s\cdot L_r\sigma}{M\cdot V_s}\cdot\dot{P}_s^{ref}+R_r\cdot I_{rq}+\\&+g\cdot w_s\cdot L_r\cdot\sigma\cdot I_{rd}+\\&+g\cdot\frac{M\cdot V_s}{L_s}+L_r\cdot\sigma\cdot v_1\cdot sgn\left(s(P)\right)\end{aligned} \tag{40}$$

$$\begin{cases}V_{rq-Equi}=-\dfrac{L_s\cdot L_r\sigma}{M\cdot V_s}\cdot\dot{P}_s^{ref}+R_r\cdot I_{rq}+\\ \qquad+g\cdot w_s\cdot L_r\cdot\sigma\cdot I_{rd}+g\cdot\dfrac{M.V_s}{L_s}\\ V_{rq-attr}=L_r\cdot\sigma\cdot v_1\cdot sgn\left(s(P)\right)\end{cases} \tag{41}$$

V.3. Reactive Power Control

The same procedure is followed to derive reactive power control law. Then, the related expressions are given below:

$$s(Q)=\left(I_{rd}^{ref}-I_{rd}\right) \tag{42}$$

$$\dot{s}(Q)=\left(\dot{I}_{rd}^{ref}-\dot{I}_{rd}\right) \tag{43}$$

By replacing $\dot{I}_{rd}^{ref}$ and $\dot{I}_{rd}$ by their relative expressions, we get:

$$\dot{s}(Q)=\begin{pmatrix}\left(\dfrac{V_s}{w_s\cdot M}-\dfrac{L_s}{V_s\cdot M}\cdot\dot{Q}_s^{ref}\right)+\\ -\dfrac{1}{L_r\sigma}\left(V_{rd}-R_r\cdot I_{rd}+g\cdot w_S\cdot L_r\cdot\sigma\cdot I_{rq}\right)\end{pmatrix} \tag{44}$$

$$\dot{s}(Q)=\begin{pmatrix}\left(\dfrac{V_s}{w_s\cdot M}-\dfrac{L_s}{V_s\cdot M}\cdot\dot{Q}_s^{ref}\right)-\dfrac{1}{L_r\sigma}V_{rd}+\\ -\dfrac{1}{L_r\sigma}\left(-R_r\cdot I_{rd}+g\cdot w_s\cdot L_r\cdot\sigma\cdot I_{rq}\right)\end{pmatrix} \tag{45}$$

$$\begin{aligned}V_{rd}=&L_r\sigma\left(\frac{V_s}{w_s\cdot M}-\frac{L_s}{V_s\cdot M}\dot{Q}_s^{ref}\right)+R_r\cdot I_{rd}+\\&-g\cdot w_s\cdot L_r\cdot\sigma\cdot I_{rq}+L_r\cdot\sigma\cdot v_2\cdot sgn\left(s(Q)\right)\end{aligned} \tag{46}$$

$$\begin{cases}V_{rd-Equi}=L_r\sigma\left(\dfrac{V_s}{w_s\cdot M}-\dfrac{L_s}{V_s\cdot M}\dot{Q}_s^{ref}\right)+\\ \qquad+R_r\cdot I_{rd}-g\cdot w_s\cdot L_r\cdot\sigma\cdot I_{rq}\\ V_{rd-attr}=L_r\cdot\sigma\cdot v_2\cdot sgn\left(s(Q)\right)\end{cases} \tag{47}$$

Explicit block diagram of sliding mode control approach applied to the DIFG is given in Fig. 10 below.

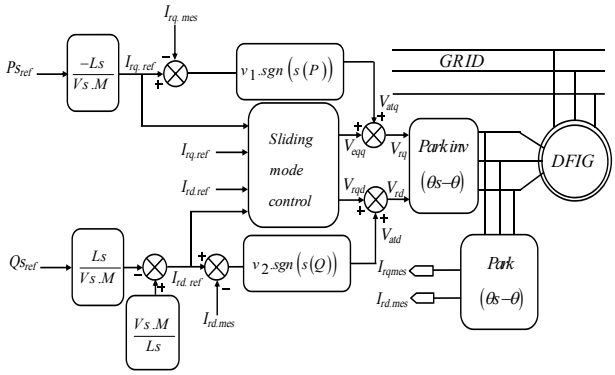

Fig. 10. Block diagram the sliding mode controller

V.4. Simulation Results

Two case studies have been studied. The first case is the implementation of the control law with a fixed speed (without turbine). While in the second case, the simulation study has been carried out with variable speed (with the presence of turbine).

Case 1: Fixed speed operation

Figs. 11 and Figs. 12 are the simulation results for active and reactive power response in case of fixed speed operation when traditional PI controller (Fig. 11(a) and Fig. 12(a)) and sliding mode control (Fig. 11(b) and Fig. 12(b)) are applied. In this case study, simulation results show clearly the improvement of active and reactive power demand obtained by applying sliding mode

control in term of time response and good reference tracking accuracy than those obtained using traditional PI regulator. We notice here, in case of step change, that the sliding mode controller transient responses of both active and reactive powers present no overshoot whereas the steady state error is close to zero.

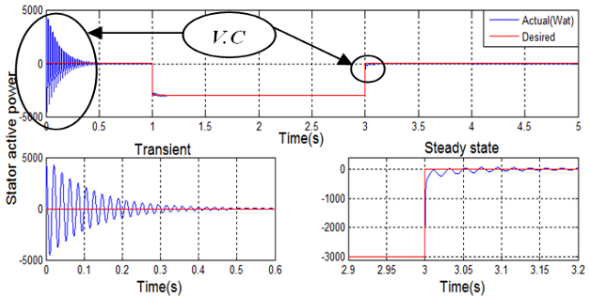

(a)

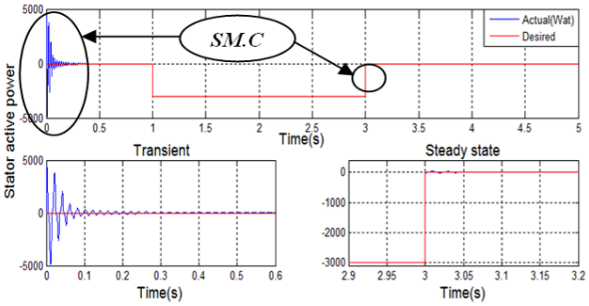

(b)

Figs. 11. Stator active power: (a) Vector control
(b) Sliding mode control

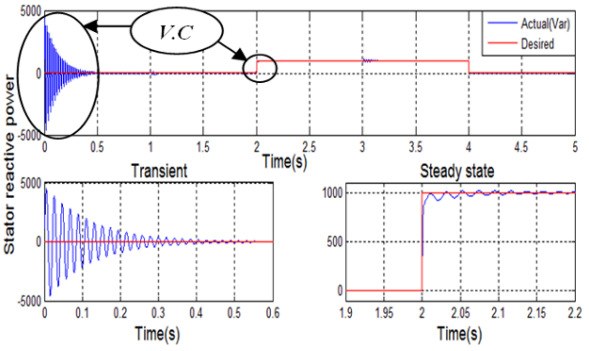

(a)

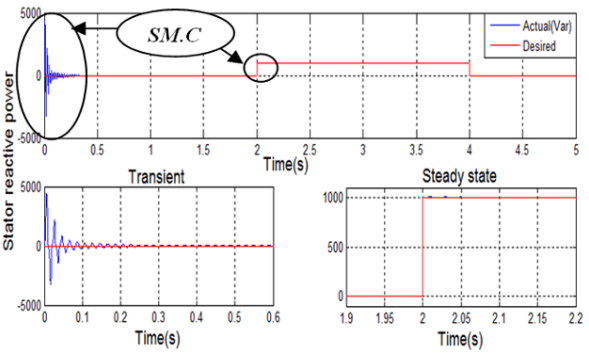

(b)

Figs. 12. Stator reactive power: (a) Vector control
(b) Sliding mode control

Case 2: Variable speed operation

In this case, the overall system consists of a DFIG controlled by a bidirectional power converter allowing the control of both active and reactive generated power.

For this purpose a wind speed profile (Fig. 13(a)) has been applied to the turbine where the generated mechanical speed is shown in Fig. 13(b). The obtained power coefficient, *Cpmax*, and the Tip speed ratio, λopt, are shown in Fig. 13(c) and Fig. 13(d) respectively.

The control goal is to control the output active power determined from the available mechanical power and reactive power in order to get unity power factor operation. The simulation results given bellow are obtained for two control strategy namely: Vector and sliding mode control respectively. Fig. 14(a) and Fig. 14(b) show the simulation results of active and reactive power for both vector and sliding mode control respectively.

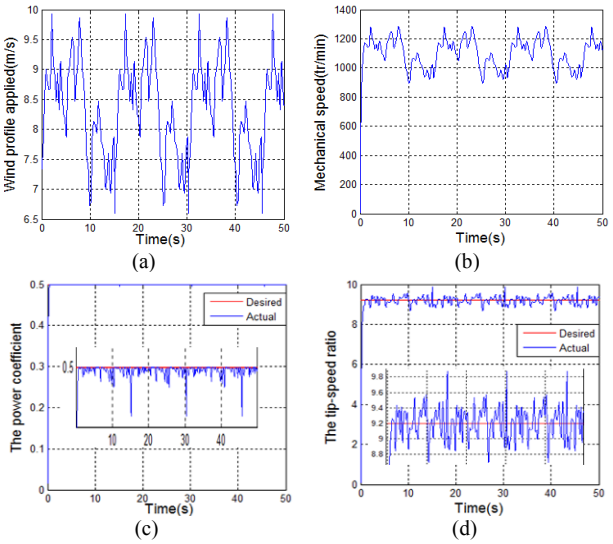

(a) (b) (c) (d)

Figs. 13. (a) Wind profil applied, (b) Mechanical speed
(c) Power coefficient, (d) Tip-speed ratio

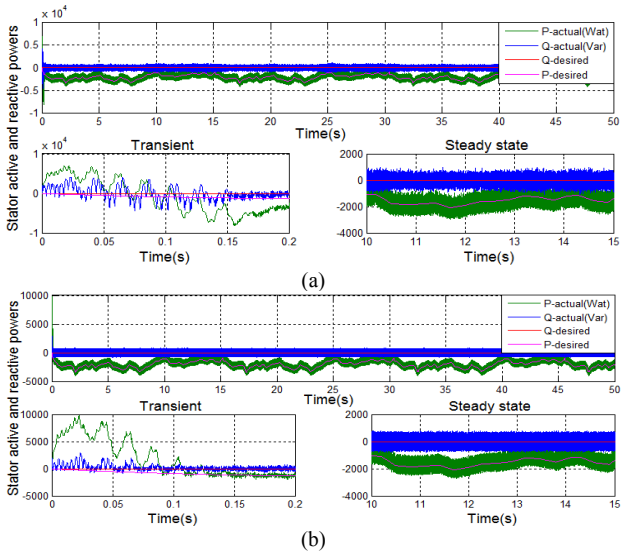

(a)

(b)

Figs. 14. Stator's active and reactive powers:
(a) Vector control, (b): Sliding mode control

First it could be noticed the best performances of sliding mode control compared to vector control in steady state as well as in transient.

In addition in case of disturbance, the simulation results of the sliding mode control show no overshoot and the overall system behaves like a first order system while in the vector control, it behaves like a second order system with a significant overshoot.

On the hand, the time response got in sliding mode control is less than obtained in vector control. In Figs. 15(a), 15(b), 16(a) and 16(b) are the time evolution of stator and rotor currents respectively in both transient and steady state.

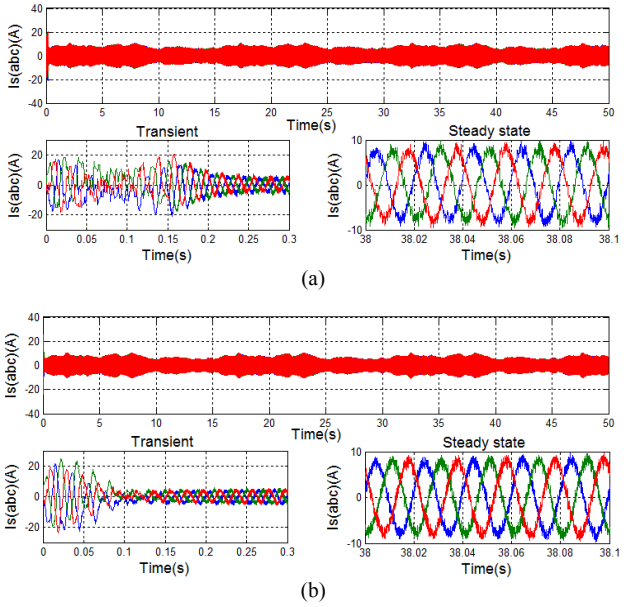

(a)

(b)

Figs. 15. Stator current components:
(a) Vector control, (b) Sliding mode control

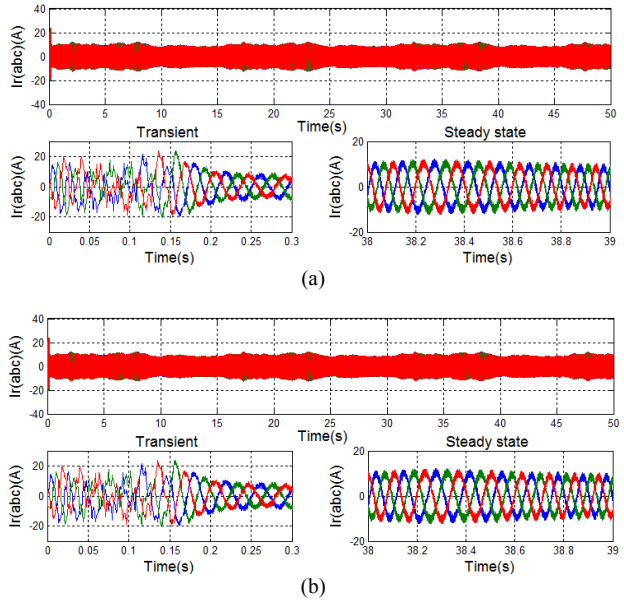

(a)

(b)

Figs. 16. Rotor current components: (a): Vector control, (b): Sliding mode control

In Figs. 17(a) and (b) it is given the time evolution of the DC voltage and phase current versus phase voltage respectively. It is clearly shown that the overall system operate at a unity power factor.

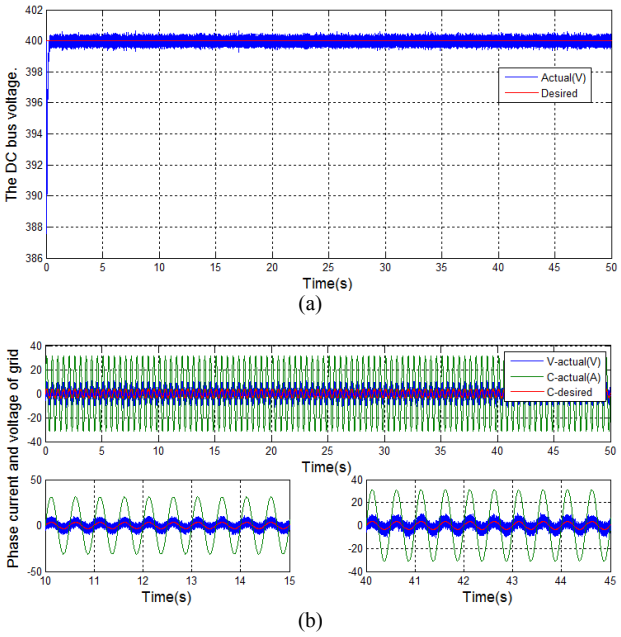

(a)

(b)

Figs. 17. (a): DC bus voltage, (b): The phase current and voltage of grid

VI. Conclusion

The present paper presents a comparative study on the performance of two control strategies; vector and sliding mode controller applied on a DFIG wind turbines when operated in power regulation mode. The comparative study has focused on the main performance parameters namely: dynamic and steady state operation. In addition, two operating mode a DFIG with fixed speed operation and linked to a turbine with variable speed operation, has been chosen to strengthen the comparative study. Both of vector and sliding mode control allow the decoupling of real and reactive power in order to be controlled separately. The simulations results have shown the effectiveness of sliding mode controller over vector control in term of dynamic and steady state operation.

The control based on sliding mode controller not only enhances the overall quality of the delivered power but also ensure functioning at unity power factor.

References

[1] Xiaohong Wang; Jinming Yang; Xianyong Zhang; Jie Wu, "Sliding Mode Control of Active and Reactive Power for Brushless Doubly-Fed Machine," *Computing, Communication, Control, and Management, 2008. CCCM '08. ISECS International Colloquium on* , vol.2, no., pp.294,298, 3-4 Aug. 2008.

[2] E. Pouresmaeil, D. Montesinos Miracle, and O. Gomis- Bellmunt. Control scheme of three-level h-bridge converter for interfacing between renewable energy resources and ac grid. In *Power Electronics and Applications (EPE 2011), Proceedings of the 2011-14th European Conference on*, pp:1–9, 30 /11-sept.1- 2011.

[3] A. Sumper, O. Gomis-Belmunt, A. Sudria-Andreu, R. Villafafila-

Robles, and J. Rull-Duran. Short-term voltage stability of fixed-speed WT: Comparison of single and double cage. *In Power and Energy Society General Meeting, 2010 IEEE*, pp: 1 –8, july 2010.
[4] O. Gomis-Bellmunt, A. Junyent-Ferre,A. Sumper, and J. Bergas-Jan. Ride-through control of a doubly fed induction generator under unbalanced voltage sags. *Energy Conversion. IEEE Transactions on*, 23(4):1036 –1045, dec. 2008.
[5] A. Junyent-Ferre, O. Gomis-Bellmunt, M. Martinez- Rojas, A. Sumper, M. Sala, and M. Mata. Digital simulations of voltage dip characteristics of wind turbine systems. In *Electrical Power Quality and Utilisation. EPQU 2007. 9th International Conference on*, 1 –6, oct. 2007.
[6] A. Sumper, O. Gomis-Bellmunt, A. Sudria-Andreu, R. Villafafila-Robles, and J. Rull-Duran. Response of fixed speed wind turbines to system frequency disturbances. *Power Systems, IEEE Transactions on*, 24(1):181 –192, feb. 2009.
[7] H. Li and Z. Chen. Overview of different wind generator systems and their comparisons. *lET Renewable Power Generation*, vol. 2, no. 2, pp.123 - 138, june 2008.
[8] hmed M. Kassem , Khaled M. Hasaneen , Ali M. Yousef . Dynamic modeling and robust power control of DFIG driven by wind turbine at infinite grid. *Electrical Power and Energy Systems* 44 (2013).pp: 375–382.
[9] Maria Letizia Corradini, Gianluca Ippoliti, and Giuseppe Orlando. Robust Control of Variable-Speed Wind Turbines Based on an Aerodynamic Torque Observer. *IEEE Trans. Control Syst. Technol.*, vol. 21, no. 4, pp: 1199–1206, July 2013.
[10] Brice Beltran, Mohamed El Hachemi Benbouzid, Senior Member, IEEE, and Tarek Ahmed-Ali. Second-Order Sliding Mode Control of a Doubly Fed Induction Generator Driven Wind Turbine. *IEEE Trans. Energy Convers*. vol. 27, no. 2, pp. 261–269, Jun. 2012.
[11] Zhankui Song, Kaibiao Sun. Adaptive backstepping sliding mode control with fuzzy monitoring strategy for a kind of mechanical system. *ISA Transactions* 53(2014), pp. 125–133.
[12] Amimeur H, Abdessemed R, Aouzellag D, Merabet E, Hamoudi F. A sliding mode control associated to the field-oriented control of dual-stator induction motor drives. *J Electr Eng* 2010; 10(3) [Art. 2]
[13] S.Abdeddaim, A.Betka, S Drid, M Becherif. Implementation of MRAC controller of a DFIG based variable speed grid connected wind turbine. *Energy Convers Manage*. 79 (2014), pp. 281–288.
[14] M.L. Corradini, G. Ippoliti, and G. Orlando. An Aerodynamic Torque Observer for the Robust Control of Variable-Speed Wind Turbines. *in 51st IEEE Conference on Decision and Control*, December 10-13, 2012. Maui, Hawaii, USA, pp. 2483 –2488.
[15] F.D. Bianchi, H. De Battista, R.J. Mantz. Wind turbine control systems, principles, Modelling and Gain Scheduling Design. Springer2007.
[16] Radia Abdelli, Djamila Rekioua, Toufik Rekioua, Abdelmounaïm Tounzi. Improved direct torque control of an induction generator used in a wind conversion system connected to the grid. *ISA Transactions* 52(2013).pp:525–538.
[17] T. Mesbahi, T. Ghennam, E.M. Berkouk. A Doubly Fed Induction Generator for Wind Stand-Alone Power Applications (Simulation and Experimental Validation) 978-1-4673-0142-8/12/$26.00 ©, pp. 2028-2033, 2012 IEEE.
[18] Yongchang Zhang, Jianguo Zhu, Jiefeng Hu. Model predictive direct torque control for grid Synchronization of Doubly Fed Induction Generator. *Proceedings of the 2011 IEEE. International Electric Machines & Drives Conference (IEMDC)* 15-18 May 2011 Niagara Falls, pp. 765 –770.
[19] Victor Flores Mendes, Clodualdo Venicio de Sousa, Selˆenio Rocha Silva, Balduino Cezar Rabelo, Jr., and Wilfried Hofmann, Senior Member, IEEE. Modeling and Ride-Through Control of Doubly Fed Induction Generators During Symmetrical Voltage Sags. *IEEE Trans. Energy Convers*., vol. 26, no.4, pp. 1161–1171, dec 2011.
[20] Esmaeil Rezaei, Ahmadreza Tabesh, Member, IEEE, and Mohammad Ebrahimi. Dynamic Model and Control of DFIG Wind Energy Systems Based on Power Transfer Matrix. *IEEE Trans. Energy Convers.* vol. 27, no. 3, pp. 1485–1493, july 2012.
[21] H.T. Jadhav, Ranjit Roy. A comprehensive review on the grid integration of doubly fed induction generator. *Int J Electr Power Energy Syst* 2013; 49(01), pp. 8–18.
[22] S. Abdeddaim, A. Betka. Optimal tracking and robust power control of the DFIG wind turbine. *Int J Electr Power Energy Syst* 2013; 49(01), pp.: 234–242.
[23] K. Ghedamsia, E.M. Berkouk. Control of wind generator associated to a flywheel energy storage system. *Renewable Energy*, Volume 33, Issue 9, pp 2145-2156, Elsevier (2008).
[24] Yong Feng; Bing Chen; Xinghuo Yu; Yongmin Yang, "Terminal sliding mode control of induction generator for wind energy conversion systems," *IECON 2012 - 38th Annual Conference on IEEE Industrial Electronics Society* , vol., no., pp.4741,4746, 25-28 Oct. 2012.
[25] Xiaohong Wang, Jinming Yang, Xianyong Zhang, and Jie Wu. Sliding Mode Control of Active and Reactive Power for Brushless Doubly-Fed Machine. *Proceedings of the 2008 IEEE. ISECS International Colloquium on Computing, Communication, Control, and Management,* pp: 294-298.
[26] Amimeur H, Aouzellag D, Abdessemed R, Ghedamsi K. Sliding mode control of a dual-stator induction generator for wind energy conversion systems. *Int J Electr Power Energy Syst* 2012; 42(01), pp: 60–70.
[27] Errami, Y.; Maaroufi, M.; Ouassaid, M., "Variable Structure Direct Torque Control and grid connected for wind energy conversion system based on the PMSG," *Complex Systems (ICCS), 2012 International Conference on* , vol., no., pp.1,6, 5-6 Nov. 2012.
[28] D. Kairous, R. Wamkeue. DFIG-based fuzzy sliding-mode control of WECS with flywheel energy storage. *Electric Power Systems Research* 93 (2012), pp. 16– 23.
[29] S. Wen, F. Wang. Sensorless Direct Torque Control of High Speed PMSM Based on Variable Structure Sliding Mode," *Proceedings of Electrical Machines and Systems, ICEMS-IEEE, International Conference on*, pp. 995 – 998. 2008.
[30] Mosayebian, M.E., Monsef, H., Reliability evaluation in power system integrated with wind power, (2010) *International Review on Modelling and Simulations (IREMOS),* 3 (3), pp. 368-372.
[31] Gopal Sharma, K., Bhargava, A., Gajrani, K., Stability analysis of DFIG based wind turbines connected to electric grid, (2013) *International Review on Modelling and Simulations (IREMOS),* 6 (3), pp. 879-887.
[32] Hamdi, N., Bouzid, A., New control of a doubly-fed induction generator of a variable speed wind turbine with Ku transformation, (2013) *International Review of Automatic Control (IREACO),* 6 (2), pp. 183-188.
[33] Beltran, B., Benbouzid, M., Ahmed-Ali, T., Mangel, H., DFIG-based wind turbine robust control using high-order sliding modes and a high gain observer, (2011) *International Review on Modelling and Simulations (IREMOS),* 4 (3), pp. 1148-1155.
[34] Moutchou, M., Abbou, A., Mahmoudi, H., Induction machine speed and flux control, using vector-sliding mode control, with rotor resistance adaptation, (2012) *International Review of Automatic Control (IREACO),* 5 (6), pp. 804-814.
[35] Abdellah, A., Abdelhafid, A., Mostafa, R., Combining sliding mode and linear quadratic regulator to control the inverted pendulum, (2013) *International Review of Automatic Control (IREACO),* 6 (1), pp. 69-76.

Authors' information

PhD student **Riyadh Rouabhi** was born in M'sila, Algeria. He received the M.Sc. degrees in Electrical Engineering from Ferhat Abbas University, Setif, Algeria, in 2012. He has been working for more than 3 years with the Department of Electrical Engineering, University of M'sila, as a Professor and Engineer laboratory. Currently. His current area of research includes design and control of doubly fed induction Generator, reliability, magnetic bearing, and renewable energy.

Pr. **Rachid Abdessemed** was born in Batna, Algeria, . He received the M.Sc. and Ph.D. degrees in Electrical Engineering from Kiev Polytechnic Institute, Kiev, Ukraine, in 1978 and 1982; respectively. He has been working for more than 30 years with the Department of Electrical Engineering, University of Batna, as a Professor. Currently, he is the Director of the Electrical Engineering Laboratory. His current area of research includes design and control of induction machines, reliability, magnetic bearing, and renewable energy.

Dr. **Aissa Chouder** received the Ingénieur in Electronics and Magister in Electronics degrees from Ferhat Abbas University, Sétif, Algeria, in 1991 and 1999, respectively, and the Ph.D. degree in electronic engineering from the Universitat Politècnica de Catalunya (UPC), Barcelona, Spain, in 2010. He is currently a Senior Researcher with the Photovoltaic Laboratory, Development Centre of Renewable Energies, Algiers, Algeria. His research interests include power electronics modeling and control for renewable energy systems.

Ali Djerioui was born in M'sila, Algeria, in 1986. In 2009,he received the engineering degree in electrical engineering from the University of M'sila, Algeria. In 2011,he was graduated M.Sc. degree in electrical engineering from the Polytechnic Military Academy in Algiers, Algeria respectively where he is currently working toward the Ph.D. degree in Electronic Instrumentation systems at the University of USTHB, Algiers, Algeria. His main interests are power converters, control and power quality.

